AIP | Applied Physics Letters

Slowing of femtosecond laser-generated nanoparticles in a background gas

C. M. Rouleau, A. A. Puretzky, and D. B. Geohegan

Citation: Applied Physics Letters **105**, 213108 (2014); doi: 10.1063/1.4902878
View online: http://dx.doi.org/10.1063/1.4902878
View Table of Contents: http://scitation.aip.org/content/aip/journal/apl/105/21?ver=pdfcov
Published by the AIP Publishing

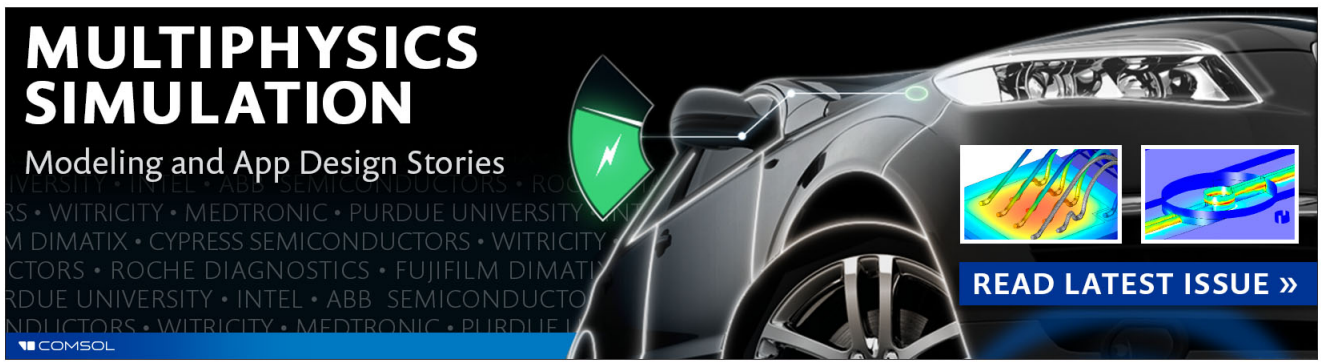

Slowing of femtosecond laser-generated nanoparticles in a background gas

C. M. Rouleau, A. A. Puretzky, and D. B. Geohegan
Center for Nanophase Materials Sciences, Oak Ridge National Laboratory, Oak Ridge, Tennessee 37831, USA

(Received 5 November 2014; accepted 16 November 2014; published online 25 November 2014)

The slowing of Pt nanoparticles in argon background gas was characterized by Rayleigh scattering imaging using a plume of nanoparticles generated by femtosecond laser through thin film ablation of 20 nm-thick Pt films. The ablation was performed at threshold laser energy fluences for complete film removal to provide a well-defined plume consisting almost entirely of nanoparticles traveling with a narrow velocity distribution, providing a unique system to unambiguously characterize the slowing of nanoparticles during interaction with background gases. Nanoparticles of ~200 nm diameter were found to decelerate in background Ar gas with pressures less than 50 Torr in good agreement with a linear drag model in the Epstein regime. Based on this model, the stopping distance of small nanoparticles in the plume was predicted and tested by particle collection in an off-axis geometry, and size distribution analysis by transmission electron microscopy. These results permit a basis to interpret nanoparticle propagation through background gases in laser ablation plumes that contain mixed components. © *2014 AIP Publishing LLC*.
[http://dx.doi.org/10.1063/1.4902878]

Understanding how nanoparticles propagate through background gases is important for many thin film and nanomaterial growth processes, especially in pulsed laser deposition, where nanoparticles comprise a significant fraction of the material ejected from a target.[1–5] Femtosecond laser irradiation of solids produces a high fraction of nanoparticles in the plume,[1,6–14] and understanding how these nanoparticles penetrate background gases is important not only for synthesis of new materials but also for laser sampling and machining.

Only a few experiments have studied the propagation of fs-laser plumes through background gases.[7,10] Collecting nanoparticles on witness plates placed at different distances from the target confirms that nanoparticles of different size have different stopping distances in a background gas, and that this can be used for size separation.[15] *In situ* plume emission studies[7,9,10] typically reveal two plume components emitted from solid targets irradiated by fs-lasers: a fast, highly forward-directed component of plasma fluorescence attributed to atoms and molecules that exhibits a plume sharpening effect similar to that observed in MALDI,[16] and a slower component of material that emits blackbody radiation which is attributed to nanoparticles. In a background gas, the two components propagate differently. The fast (atomic/molecular) component becomes rapidly slowed to nearly stop, and the slow (nanoparticle) component overtakes it to propagate to longer distances.[16] Tracking nanoparticle propagation in these studies is complicated by this overlap of plume components, by the generation of new nanoparticles by condensation of the atomic/molecular component, and by the lifetimes of the plasma fluorescence and the blackbody radiation due to thermalization in the background gas.

Recently, we showed that near-threshold through thin film ablation (TTFA) of nanometers-thin Pt films in a low fluence regime produces a compact plume composed nearly entirely of hot nanoparticles that we imaged using their nascent blackbody emission.[17] Unlike previous studies, the compact plume displayed a well-defined velocity distribution wherein the trailing edge velocity was comparable to that of the leading edge, and the plume itself was observed to rebound off of donor and receiver surfaces, indicating that witness plates may not provide accurate nanoparticle size distributions.

Here, we utilize this well-defined velocity distribution of Pt nanoparticles to unambiguously understand how they propagate and slow in background gases, and we employ Rayleigh scattering imaging as a diagnostic to follow the nanoparticles long after they have cooled.

As shown in Figure 1 and described in Ref. 17, 20 nm-thick films of Pt were e-beam evaporated onto 1.5 mm-thick fused silica substrates and ablated from the backside using single fs-laser pulses (Coherent Legend HE, 800 nm, 40 fs, 40–60 mJ/cm^2, 20 × 25 μm^2). A sheet beam from a second laser (Quanta Ray DCR-11, 355 nm, 8 ns) was brought to a 1 cm-long line focus and oriented to intersect the ejecta in front of the target. Rayleigh scattering (RS) imaging was recorded at different time-delays with respect to the ablation beam by a gated, intensified CCD (ICCD) camera, mounted

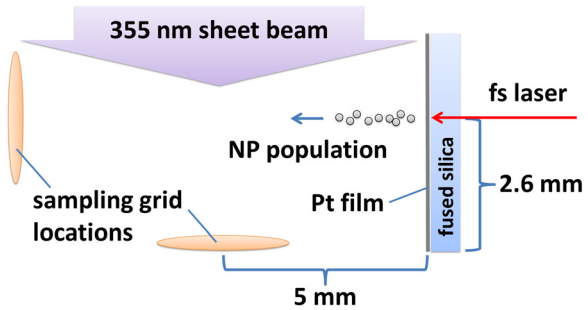

FIG. 1. Schematic of experimental setup showing orientation of fs laser beam, thin film target and fused silica host substrate, sheet laser beam for Rayleigh scattering, and axis of nanoparticle propagation. ICCD camera (not shown) was oriented normal to the page for side-on imaging. For nanoparticle sampling, lacey-carbon coated TEM grids were oriented and placed in one of the two locations shown.

orthogonal to both laser beams. A fresh Pt region was used for every laser shot. Nanoparticle sizes collected on lacey carbon TEM grids placed in one of two sampling locations (shown in Fig. 1) were measured by a Libra 120 transmission electron microscope.

Fig. 2(a) shows selected RS-ICCD images collected during the first 100 μs following TTFA of 20 nm-thick Pt films in vacuum, and in 12.8, 25.5, and 51.7 Torr Ar. Most notable is the formation of a highly forward-directed, compact plume, which, contrary to plumes observed from bulk targets, had a trailing edge velocity that was comparable to that of the leading edge. More interesting, however, was the progressive slowing that occurred as the Ar pressure in the processing chamber was increased, until finally at 51.7 Torr the ejecta was observed to "stop" approximately 5 mm from the surface of the target after ~100 μs. After stopping, the plume remained stationary and could be observed for nearly 2 s until the nanoparticles diffused away.

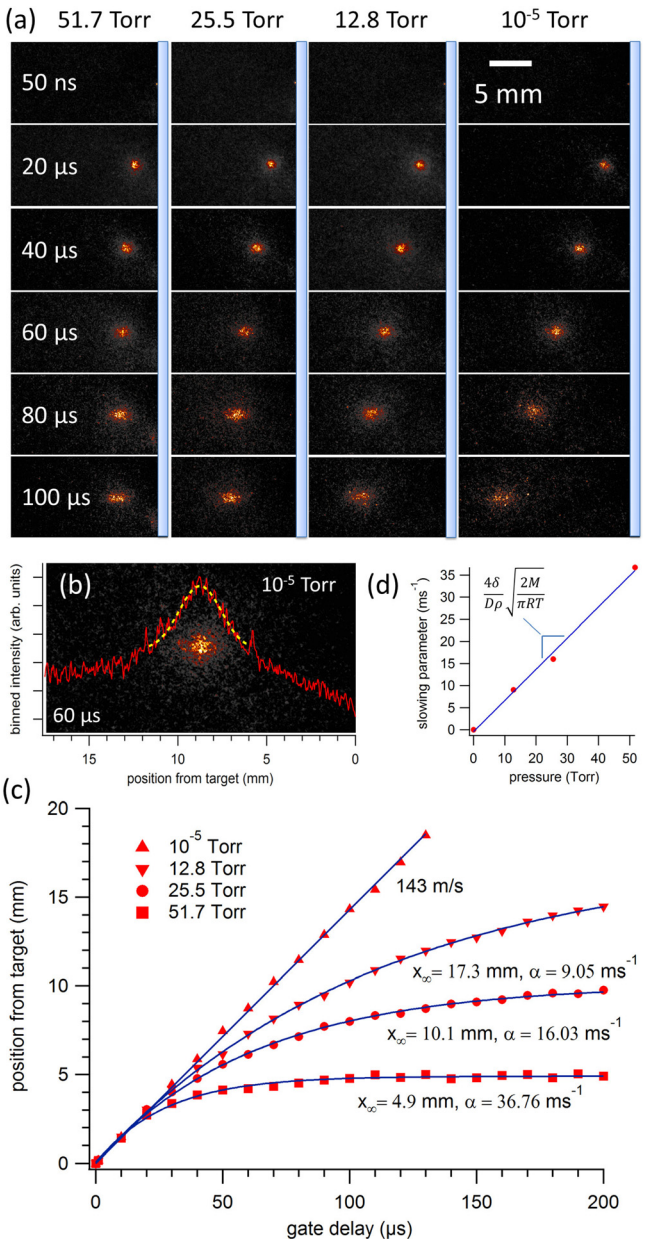

FIG. 2. (a) Side-on ICCD images (50 ns-gate) of Rayleigh-scattered light from a packet of nanoparticles at the indicated times after fs-laser ablation of 20 nm-thick Pt films in background Ar at the indicated pressures. (b) Example of image intensity binning to determine a line profile, which is curve-fit to determine the plume centroid. (c) R-t plot of the plume centroids along the target surface normal in vacuum, and Ar pressures of 12.8, 25.5, and 51.7 Torr. The blue lines represent fits of Eq. (3) to the experimental data. (d) Slowing parameters, α, derived from the curve fits in (c).

Plots of the nanoparticle slowing dynamics were made by analyzing the RS-ICCD images as shown in Fig. 2(b), with the resultant centroid of each image along the target surface normal plotted for the different background pressures as shown in Fig. 2(c). The propagation dynamics for the nanoparticle plumes were fit, for the reasons described below, with a model involving a drag force that had a *linear* dependence on particle velocity.

A spherical particle of radius, r, moving within a stationary gaseous medium with mean free path, λ, can be expected to slow from the collective effects of collisions with individual gas molecules when $r \ll \lambda$, in the particle regime, by the Epstein drag force. Alternatively, when $r \gg \lambda$, particle slowing results from a frictional force exerted by a viscous fluid, in the fluid regime, by the Stokes drag force.[18,19] Stokes and Epstein drag forces can be shown to be equal when $r = 9/4\ \lambda$, formally defining a transition point.[19] In all of the experiments here, $r < 9/4\ \lambda$ since the largest r measured was 0.15 μm and the smallest λ (at $P_{Ar} = 51.7$ Torr) was ~1.2 μm (kinematic diameter of Ar taken as in Ref. 20). Slowing is predicted to result from collisions between individual nanoparticles and molecules by the Epstein drag force.

The Epstein drag force is linear with the relative velocity between the particle and the gas, and is expressed as shown in Eqs. (1) and (2) for the equations of motion expected for a spherical particle in our experiments.

$$m_p \frac{d^2x}{dt^2} = -\frac{4}{3}\pi\delta n m_g \hat{c} r^2 \upsilon_{rx}, \tag{1}$$

$$m_p \frac{d^2y}{dt^2} = -\frac{4}{3}\pi\delta n m_g \hat{c} r^2 \upsilon_{ry} + m_p g. \tag{2}$$

Here, x and y are the positions of the particle along the surface normal of the target and in the direction of gravity, respectively, m_p and m_g are the respective masses of the particle and the gas molecules, n is the number density of the gas, $\hat{c}$ is the mean thermal velocity of the gas, v_r is the relative velocity between the particle and gas, r is the particle *radius*, g is the acceleration of gravity, and δ describes the interaction between the particle and a gas molecule, which was assumed to be close to $1 + \pi/8$ for metallic particles.[19] Assuming the gas is essentially stationary, $v_{rx} \approx dx/dt$ and $v_{ry} \approx dy/dt$, and the solutions to Eqs. (1) and (2) can be written as shown in Eqs. (3) and (4), where x_∞ is the position at which the particle comes to a stop and the slowing parameter, α, is as shown. Note that the initial velocity of the particle, $v_o = \alpha \cdot x_\infty$,

$$x(t) = x_\infty(1 - e^{-\alpha t}), \tag{3}$$

$$y(t) = \frac{g}{\alpha}\left(t - \frac{1}{\alpha}\right)(1 - e^{-\alpha t}), \tag{4}$$

$$\text{where } \alpha = \frac{4}{3}\pi\delta n \frac{m_g}{m_p}\hat{c} r^2.$$

To make fitting of the experimental data more convenient, α was recast as shown in Eq. (5), where P is the gas pressure, D is the particle *diameter*, ρ is the density of the particle, M is the molar mass of the gas, R is the gas constant, T is the gas temperature, and all other values are as before,

$$\alpha = \frac{4\delta P}{D\rho}\sqrt{\frac{2M}{\pi RT}}. \quad (5)$$

Note that ρ in Eq. (5) requires some consideration as it is dependent on the temperature of the particle. A reasonable estimate here is based on our recent finding that Pt particles are nearly molten during fs ablation of thin Pt films, with temperatures as high as 1700 K being measured 50 μs after ablation of a 20 nm Pt film.[17] At this temperature, the expansion of Pt is slightly more than 1.5%,[21] making the density only $\sim$1 mg/cm^3 lower than the room temperature value of $\sim$21.5 mg/cm^3, so particle density was regarded as a constant in our fits.

Recognizing that the plume showed no collective displacement in the y direction for the gate delays used here, Eq. (4) was ignored temporarily, and only Eq. (3) was applied to fit the experimental data in Fig. 2(c). As shown in Fig. 2(d), α was linear with pressure with a slope of 0.707 ± 0.0333 ms^{-1}/Torr, indicating that nanoparticle size, D, did not vary systematically with pressure as would be the case if aggregation and/or condensation were occurring. Using this slope, and a density of 21 mg/cm^3, a particle size range of 161 ± 7.6 nm was calculated.

To understand the nascent nanoparticle size distribution produced by TTFA in vacuum, nanoparticles were collected on a TEM grid placed 9 mm along the target surface normal as shown in Fig. 1. Figures 3(a) and 3(b) show representative TEM images of the particle morphologies and the resulting diameter range, which exhibits two components. The 161 ± 7.6 nm particle diameter resulting from the analysis of the slowing data in Fig. 2 agree within 1 standard deviation of the mean (191 ± 40.1 nm) of the broad second component in the particle size distribution shown in Fig. 3(b). This strongly indicates that, as expected, the RS images in Fig. 2(a) primarily follow the propagation of nanoparticles found in the second mode of the particle size distribution, the behavior of which in a background gas is well-described by a mean particle diameter because of the compact nature of the plume. Indeed, placing witness plates at locations both within and beyond the measured stopping distances x_∞ resulted in measurable or undetectable nanoparticle deposits, respectively.

The pressure-dependent data of Fig. 2 and the theoretical framework of Eqs. (1)–(5) suggest methods to selectively collect and size-separate as-synthesized nanoparticles generated under these unique conditions. Since α in Eq. (5) is a function of P/D, the stopping distance $x_\infty = v_o/\alpha$ for particles of diameters different than the nominal 161 nm measured in Fig. 2 should be predictable by reducing the pressure proportionately. For example, assuming the $\sim$10 nm particles from the distribution shown in Fig. 3(b) were launched with the same initial velocity, for them to just stop at a distance of 4.9 mm as in Fig. 2(d), the Ar pressure should be reduced by a factor of 10/161 from 51.7 Torr to 3.2 Torr. However, at 3.2 Torr the stopping distance for large particles is far greater than 4.9 mm (see Fig. 2), so the off-axis grid location shown in Fig. 1 was chosen to allow the highly forward directed large particles to bypass the collection grid, while the smaller *stopped* particles were allowed to freefall onto the grid via gravity between laser shots.

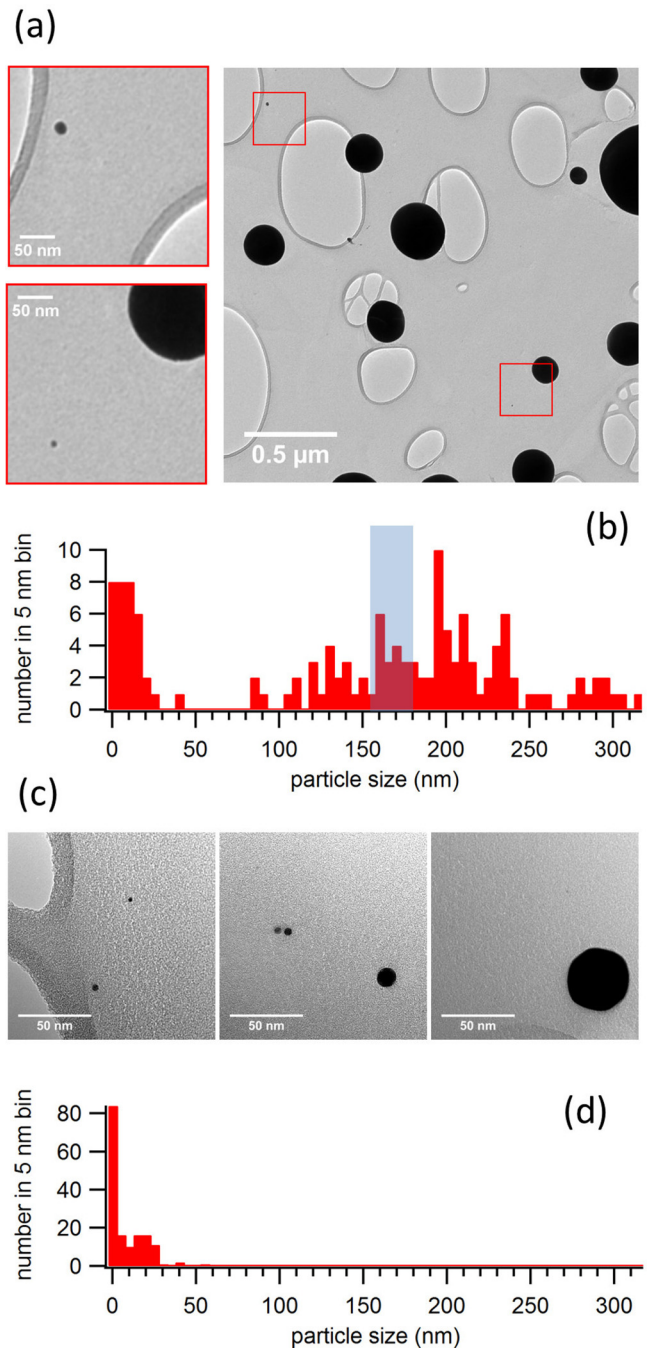

FIG. 3. TEM images and particle size distributions of Pt nanoparticles collected on lacey carbon TEM grids following 40 fs-laser ablation of 20 nm-thick Pt films on fused silica (after 4000 single shots at unique film locations). (a) and (b) Nanoparticles collected in vacuum on a vertical TEM grid positioned on-axis and 9 mm from target, exhibit a *bimodal* particle size distribution. The size range predicted from the drag model analysis is shaded in blue. (c) and (d) Nanoparticles collected in 3.2 Torr Ar by a horizontal TEM grid positioned 2.6 mm off-axis and 5 mm from target (see Fig. 1) exhibit a *unimodal* particle size distribution.

Using Eq. (4), and the dimensions shown in Fig. 1, the time required for a 10-nm particle to fall 2.6 mm is predicted

to be 11 s. Therefore, a dwell time of 15 s was used between the ~4000 laser shots. Representative nanoparticles collected are shown in Fig. 3(c) and a size distribution is shown in Fig. 3(d). The measurements indicate that the very small mode of nanoparticle diameters measured in Fig. 3(b) are separable with the appropriate choice of background pressure, and appear to follow predicted trajectories resulting from a similar initial velocity as the much larger nanoparticles imaged by RS in Fig. 2.

In summary, near-threshold fs-TTFA of nm-thick metal films provided a unique ablation plume of nanoparticles, free of plasma emission, and condensation effects, to understand how laser-generated nanoparticles slow in background gases—providing key knowledge to understand and predict nanoparticle propagation relevant to pulsed laser deposition, laser sampling of surfaces, and nanomaterial synthesis. ICCD-imaging of Rayleigh scattered light, using a time-delayed sheet of laser light, provided selectivity compared to typical blackbody emission studies, imaging primarily larger nanoparticles of Pt penetrating Ar backgrounds. A comparison of R-t plots of the propagation dynamics and TEM analysis of the collected nanoparticles show that the nanoparticle slowing is in good agreement with a linear drag model in the Epstein regime, with ~160 nm-diameter nanoparticles penetrating Ar pressures of ~10 Torr to distances of ~20 mm, and 10 nm-diameter nanoparticles penetrating Ar pressures of ~3 Torr to distances of ~5 mm. Based on this model, the stopping distances of arbitrary diameter nanoparticles in the plume can be predicted and used for size separation, as demonstrated. These results permit a basis to interpret nanoparticle propagation through background gases in laser ablation plumes that contain both nanoparticle and plasma components.

The authors gratefully acknowledge technical assistance by P. H. Fleming. This work was supported by the U.S. Department of Energy, Office of Science, Basic Energy Sciences (BES), Materials Sciences and Engineering Division and performed in part as a user project at the Center for Nanophase Materials Sciences, which is a DOE Office of Science User Facility.

[1]C. Boulmer-Leborgne, R. Benzerga, and J. Perriere, in *Laser-Surface Interactions for New Materials Production*, edited by A. Miotello and P. M. Ossi (Springer-Verlag, Berlin, 2010), Vol. 130.
[2]P. M. Ossi, in *Laser-Surface interactions for New Materials Production*, edited by A. Miotello and P. M. Ossi (Springer-Verlag, Berlin, 2010), Vol. 130.
[3]D. B. Geohegan, A. A. Puretzky, C. Rouleau, J. Jackson, G. Eres, Z. Liu, D. Styers-Barnett, H. Hu, B. Zhao, I. Ivanov, and K. More, in *Laser-Surface Interactions for New Materials Production*, edited by A. Miotello and P. M. Ossi (Springer-Verlag, Berlin, 2010), Vol. 130.
[4]D. B. Geohegan, A. A. Puretzky, M. Yoon, G. Eres, C. Rouleau, K. Xiao, J. Jackson, J. Rwadle, M. Regmi, N. Thonnard, G. Duscher, M. Chisholm, and K. More, in *Lasers in Materials Science*, edited by M. Castillejo, P. M. Ossi, and L. Zhigilei (Springer International Publishing, Switzerland, 2014), Vol. 191.
[5]P. M. Ossi, N. R. Agarwal, E. Fazio, F. Neri, and S. Trusso, in *Lasers in Materials Science*, edited by M. Castillejo, P. M. Ossi, and L. Zhigilei (Springer International Publishing, Switzerland, 2014), Vol. 191.
[6]S. Noel, J. Hermann, and T. Itina, Appl. Surf. Sci. **253**(15), 6310 (2007).
[7]S. Amoruso, R. Bruzzese, X. Wang, and J. Xia, Appl. Phys. Lett. **92**(4), 041503 (2008).
[8]S. Amoruso, N. N. Nedyalkov, X. Wang, G. Ausanio, R. Bruzzese, and P. A. Atanasov, J. Appl. Phys. **110**(12), 124303 (2011).
[9]S. S. Harilal, N. Farid, A. Hassanein, and V. M. Kozhevin, J. Appl. Phys. **114**(20), 203302 (2013).
[10]N. Farid, S. S. Harilal, H. Ding, and A. Hassanein, Appl. Phys. Lett. **103**(19), 191112 (2013).
[11]N. Tsakiris, K. K. Anoop, G. Ausanio, M. Gill-Comeau, R. Bruzzese, S. Amoruso, and L. J. Lewis, J. Appl. Phys. **115**(24), 243301 (2014).
[12]S. Amoruso, N. N. Nedyalkov, X. Wang, G. Ausanio, R. Bruzzese, and P. A. Atanasov, Thin Solid Films **550**, 190 (2014).
[13]G. O'Connell, T. Donnelly, and J. G. Lunney, Appl. Phys. A **117**, 289 (2014).
[14]I. Mirza, G. O'Connell, J. J. Wang, and J. G. Lunney, Nanotechnology **25**(26), 265301 (2014).
[15]S. C. Tseng, C. C. Yu, D. C. Lin, Y. C. Tseng, H. L. Chen, Y. C. Chen, S. Y. Chou, and L. A. Wang, Nanoscale **5**(6), 2421 (2013).
[16]A. A. Puretzky, D. B. Geohegan, G. B. Hurst, M. V. Buchanan, and B. S. Luk'yanchuk, Phys. Rev. Lett. **83**(2), 444 (1999).
[17]C. M. Rouleau, C. Y. Shih, C. Wu, L. V. Zhigilei, A. A. Puretzky, and D. B. Geohegan, Appl. Phys. Lett. **104**(19), 193106 (2014).
[18]S. J. Weidenschilling, Mon. Not. R. Astron. Soc. **180**(1), 57 (1977).
[19]P. S. Epstein, Phys. Rev. **23**, 710 (1924).
[20]K. S. W. Sing and R. T. Williams, Part. Part. Syst. Char. **21**(2), 71 (2004).
[21]R. K. Kirby, Int. J. Thermophys. **12**(4), 679 (1991).